


# Design and Development of a Mobile Sit-to-Stand Assistive Device

Satyajit Halder<sup>1</sup> · Sourav Rakshit<sup>1</sup> 

Received: 25 October 2023 / Accepted: 11 January 2024 / Published online: 12 March 2024  
© The Institution of Engineers (India) 2024

**Abstract** This work presents the design and development of an assistive device to enable natural sit-to-stand motion for individuals with lower extremity weakness. The device is conceptualized based on the synthesis of a four-bar linkage using the Burmester curve theory, the coupler of which follows the elbow trajectory of the user during sit-to-stand motion. The four-bar mechanism is incorporated in a frame that ensures stability during STS and has multiple support locations for easy and comfortable STS transfer of the user. The STS device is portable and actuated by a pair of battery-operated linear actuators enabled with a switch operated by the user. The STS device is fabricated using extruded aluminium profiles which makes it lightweight, modular for easy assembly, and adjustable to different users. The device is tested on a number of healthy subjects for whom the ground reaction forces (GRF) during STS are compared with and without using the device. Approximately 45% reduction of GRF was noted while using the STS device. Further a dynamics based optimization model was created to calculate the forces at the various support points where the user comes in contact with the STS device. The results of optimization model were compared with an experiment and found to be within 10% of experimental data. The designed and developed STS device has potential of becoming a commercial product.

**Keywords** Four-bar mechanism · Burmester curve · Trajectory optimization · Activities of daily living (ADL) · Ground reaction force (GRF)

---

✉ Sourav Rakshit  
srakshit@iitm.ac.in

<sup>1</sup> Mechanical Engineering Indian Institute of Technology, Chennai 600036, Tamilnadu, India

## Introduction

According to the Population Census 2011, nearly 104 million elderly people (aged 60 years or older) are in India; 53 million are women and 51 million are men, is given in an article by Kumar [23]. The old-age dependency ratio climbed from 10.9% in 1961 to 14.2% in 2011 and is projected to increase to 15.7% and 20.1% in 2021 and 2031, respectively for India as a whole. The healthcare service for the elderly is a critical issue with a growing elderly population. Most elderly people lose muscle strength due to ageing, and some lose natural body movement due to disease or accidents.

Sit-to-stand (STS) is one of the physical activities of daily living (ADL) and is significantly affected by ageing, overweight, and traumatic injuries, posing a major concern. Trinkoff et al. [36] studied that this problem also impacts care providers, as patient care tasks have been identified as the main cause of musculoskeletal disorders among nursing professionals. While various approaches, such as functional neuromuscular stimulation, have been attempted to address this issue, assistive mechanical and robotic devices are more commonly employed. However, many existing devices focus only on assisting with sit-to-stand motion, leaving users dependent on additional aids for walking and stabilization. Wolferts [39] designed a holder for a walker that ensures a secure and stable transfer of the patient from bed to a walker or vice-versa. Bratton [7] developed a patient riser that provides lateral support when standing up from a seated position. Wilson [38], Boyce and Boyce [6], Cunningham [10], Randall and Gill [32], and Howle [19] designed assistive devices that helps the patient to stand up. All of these devices have a common feature that the patient has to apply effort during stand-up. Kauffman [20] designed an assistive device for lifting and lowering a person and

providing support during an upright standing position. This is an electrically operated device. Vanzant [37] designed a pneumatic STS device that has an inflatable bag with two or more cavities that inflate sequentially to stabilize the person as the person is raised from or lowered into a chair. Costello [9] designed and developed an assisting lifting, standing and walking device to lift severely disabled, elderly or other physically challenged persons from a wheelchair or seated position. The lifting mechanism is actuated using a hydraulic jack. A special full-body support harness is provided with the device, which has long thigh wraps and a wide lumbar belt. Hakamiun et al. [18] developed an apparatus with a sling assembly that provides major support to the person. Marcoux and Veilleux [25] designed a lift chair with a stationary base section and a motorized lift mechanism. Fattah et al. [15] presented a passive gravity-balanced device that maintains body equilibrium during STS motion. The device has an external body weight support that increases overall weight and limits its mobility function. Peshkin et al. [29] developed a robotic device for gait and balance training. The device has a harness, a mobile base, and a post. A patient lift and transfer device was designed by Bostelman et al. [5] that has a motorized wheel and steering mechanism for driving. The device acts like a forklift mechanism. Razon [33] designed a stand-up and sit-down walker with a mounted seat. This device is actuated by a gas spring and provides partial support during standing. Kim et al. [22] designed an indoor walker using a pneumatic cylinder and a gas spring. It assists the patient by following the traditional patient transfer strategy. The patient holds the gripper attached to the lifting post of the mechanism, and for more support, a harness is wrapped around the waist. Another prevalent category of mobility aids include wheelchairs, which are designed to assist users during standing. In these devices, a mechanism is integrated into the wheelchair, extending vertically in alignment with the user, facilitating the act of standing. The primary benefit of this type of equipment is that the user can utilize it without needing external help. Goher et al. [17] presented a wheelchair that can be used as an STS assistive device, which was designed based on the same concept. Another similar device was developed by D'Angelo et al. [14]. This device has a four-bar mechanism actuated by an actuator and transforms the wheelchair to a standing position. Abdul Ghani and Tokhi [1] introduced a wheelchair designed to achieve sit-to-stand conversion. Once in an upright position, this wheelchair functions as a two-wheeled mobility aid. However, the process of sit-to-stand transformation does not provide optimal comfort to the user.

An issue commonly observed in various types of sit-to-stand (STS) devices is the discomfort that users experience during the transformation process. This discomfort arises when the elevation of the user does not align with their

natural posture and movement during the transition. To address this, recent advancements in STS technology have focused on creating movement patterns that mimic natural motions. This approach involves carefully selecting support points and designing devices that replicate optimal natural movements. Nuzik et al. [24, 28] determined the ideal posture and movement for STS transitions by capturing joint movements on photographic film. Furthermore, it has been observed that maintaining hip and shoulder movements while transitioning from a sitting position to a standing position is very important. Therefore, the proposed device is specifically designed to support the arms, shoulders, and hips during STS motion. Chugo et al. [8] designed a walker that supports the arms. This device is actuated by three actuators. Kim et al. [21, 22] designed smart mobile walker which also provides support to the arms. This device has six linear actuators, two DC hub motors and two servo motors and follows the natural STS trajectory. Asker et al. [2–4] designed and developed an assistive device based on four linear actuator-based parallel manipulator. This device supports the user at the shoulder. Rea et al. [34] proposed a method to generate trajectories using users' physical dimensions and designed a STS assistive device. Purwar et al. [30] developed an assistive device based on a six-bar mechanism, which is designed to follow the elbow trajectory.

The main disadvantage of these devices is that a full body harness is required, which makes the user uncomfortable, and these are very costly and not available in the Indian market. The devices available in the Indian market do not follow the natural STS trajectory. Most of these devices require a caregiver, making the user dependent on others. Also, nurses and caregivers working in hospitals and care facilities and involved in physically aiding of sit-to-stand of other people can develop musculoskeletal disorders themselves. Davis and Kotowski [12] studied this situation and explained it in their article. Taking this as our motivation, we designed and developed a modular STS assistive device that can be used without help of third party. This device follows a natural STS trajectory and provides multiple support to the user such that loads are distributed. The device is adjustable according to the user's height. To meet all specifications for designing the STS assistive device, first, we extracted STS data from experiments, and then we formulated the motion generation problem as four-position synthesis problem. Then, using optimization, we solved the support reaction forces.

Rest of the paper is organized as follows. Section 2 explains synthesis of the four-bar mechanism that is used for following the STS trajectory of the user. Section 3 proposes the optimization model that is used for calculating the contact forces between the user and the STS device and also the torque loads on user's body. Section 4 presents the design and fabrication details of the STS device. Section 5

presents the optimization model-based simulation and sit-to-stand experiment results. Finally, the paper ends with a discussion and concluding remarks.

### Design Conceptualization

As stated, the objective is to design and develop a compact, lightweight, user-friendly sit-to-stand (STS) and walking aid device that is portable and can be operated independently. This device is designed for elderly and disabled people, aiming to assist them in effortlessly transitioning between sitting and standing positions. Additionally, the device should provide stability and prevent falls during walking. In the following sections, we conceptualize the device and development processes as well as assist in walking. In this procedure, we studied the STS motion of healthy volunteers, collected the STS transfer data, and formulated a motion generation problem to synthesise the mechanism.

### Motion Synthesis from STS Trajectory Data

An STS experiment was conducted involving 10 healthy male volunteers aged between 20 and 27 with heights ranging from 1.55 m to 1.80 m. The selection of individuals for the trial was based on the availability of voluntary subjects. In the experiments, participants were asked to sit on an armless chair. The seated height of the chair is 450 mm above the floor. Participants were asked to keep their trunks vertically straight and arms in natural posture as shown in Fig. 1. The natural STS motion takes 2 --3 s approximately to complete the sit-to-stand transfer. The complete STS motion is classified into three phases, as

shown in Fig. 1. In phase 1, body weight transfers to the leg and starts trunk and knee flexion. In phase 2, the transition starts with the onset of knee extension and concludes with the switch from trunk flexion to trunk extension. In this phase, the contact between the seat and hip is lost. Full hip and knee extension is achieved in phase 3. During the experiment, the subjects were instructed to remain sitting before being instructed to stand up from their seats. The first step is motion tracking, carried out without obstructing a person’s movement. PhaseSpace@motion capture system was used to record the STS motion transfer data. Six markers were placed on the bony landmarks, i.e., ankle, knee, hip, shoulder, elbow, and wrist, on the body to capture joint trajectories. Four markers were placed on the chair to record the sitting position. The marker positions are shown in Fig. 2a. The natural STS trajectory for each joints are shown in Fig. 2b. The elbow trajectories of 10 volunteers is shown in Fig. 3a which shows no specific trend. Due to variations in anthropometric characteristics and individuality of motion patterns due to personality, age, weight, muscularity, etc., the STS study and the formulation of the motion synthesis problem becomes challenging. The multiple variables that affect these variances are too numerous to be managed. Thus, in this situation, we concentrate on designing a representative STS transfer assistance mechanism that can be customized according to the user. In this work, we used an actual STS trajectory of the tallest person to design the STS device, as it covers all the motion trajectories of shorter height subjects. The elbow trajectory of the tallest person is shown in Fig. 3b and four positions  $P_1, P_2, P_3, P_4$  are selected such that the original elbow trajectory can be closely generated by fitting cubic splines through these four points. These positions are shown in Table 1.

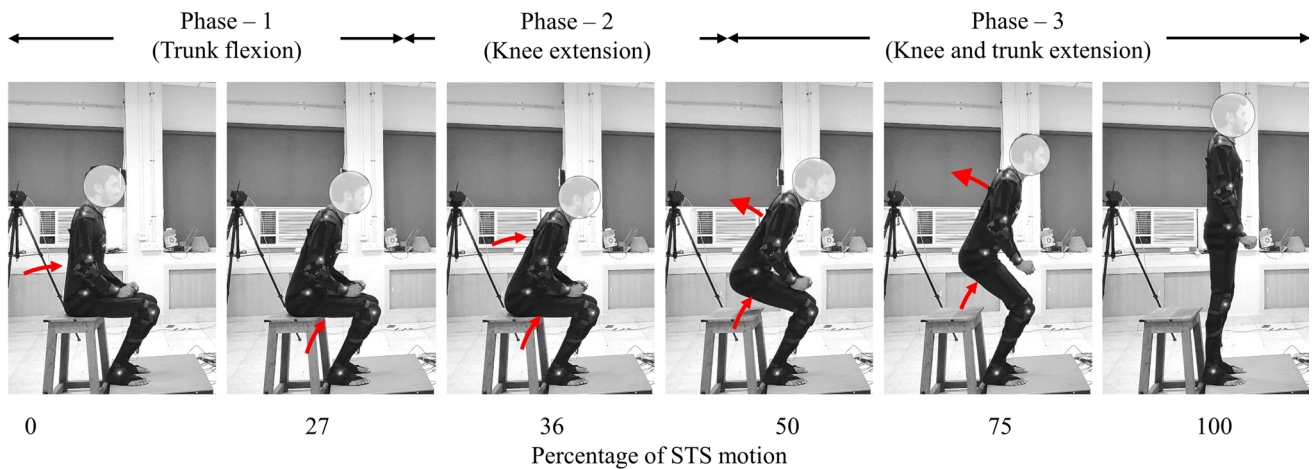
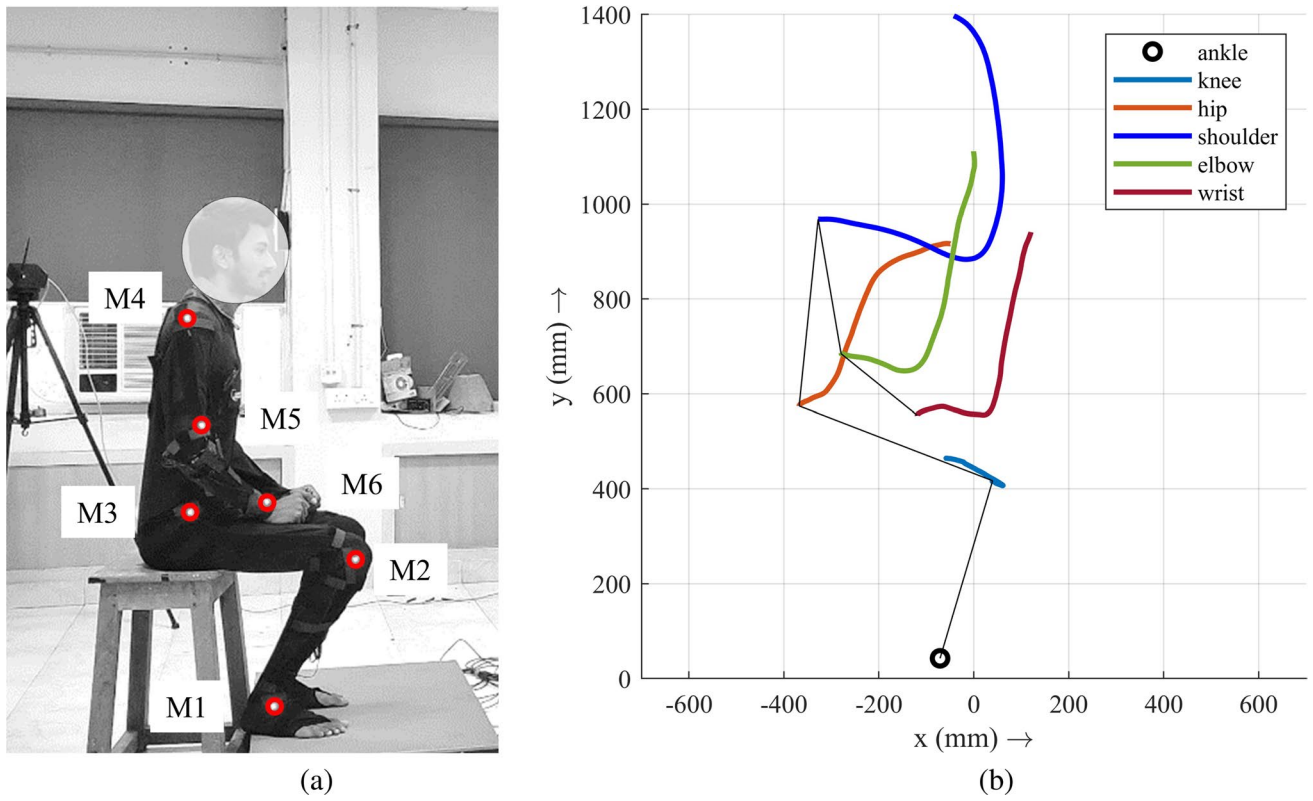
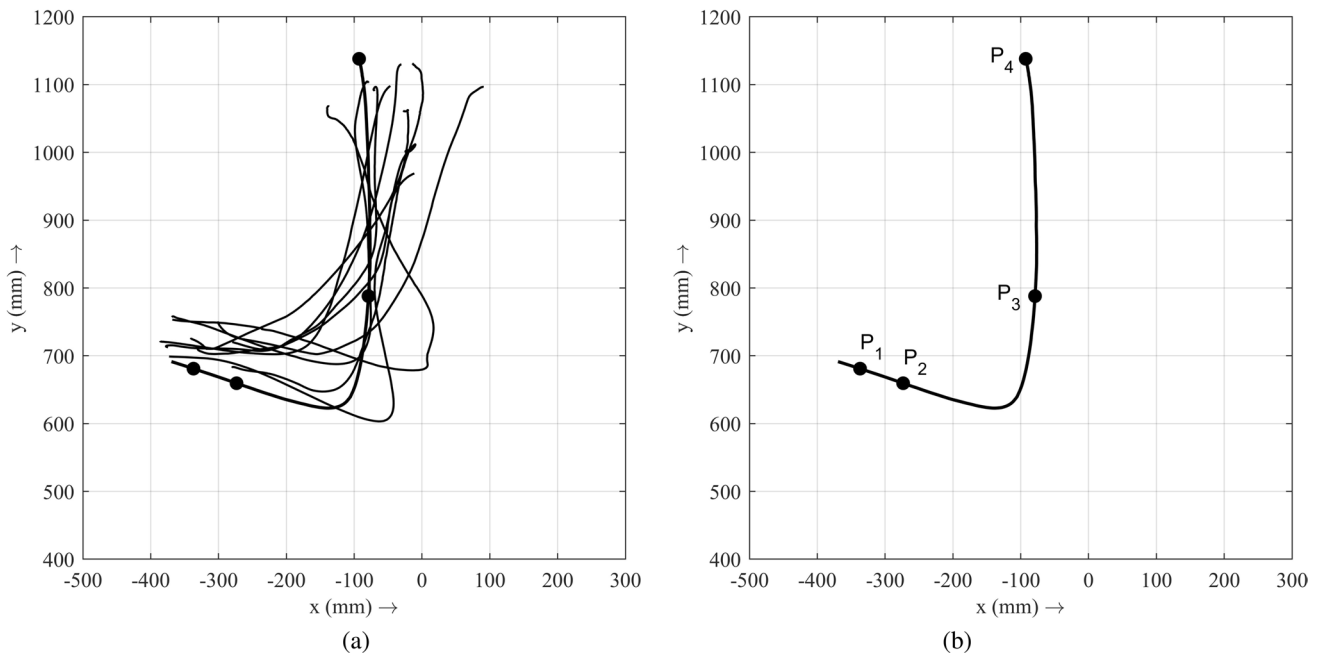


Fig. 1 Three phases of sit-to-stand (STS) motion



**Fig. 2** **a** Placement of marker for STS experiments: M1-attached at lateral malleolus, M2-attached at the knee, M3-attached at ilium, M4-attached at acromion, M5-attached at elbow, M6-attached at the wrist. **b** Joint trajectories corresponding to different markers



**Fig. 3** **a** Elbow trajectories of different individuals from motion capture experiments. The dots show the precision points for four-bar synthesis. **b** Chosen trajectory for STS-device four-bar linkage design.

The four chosen precision points  $P_1$ ,  $P_2$ ,  $P_3$ , and  $P_4$  for the synthesis procedure are shown on the trajectory

**Table 1** Precision points and coupler orientations for the four-bar

Position	STS data coordinates		Updated position	Synthesized coordinates	
	X	Y		X	Y
$P_1$	-336.9	681.0	$P_1$	-336.9	681.0
$P_2$	-273.4	659.5	$P_2$	-273.9	664.0
$P_3$	-78.9	788.0	$P_3$	-74.9	790.0
$P_4$	-92.7	1138.0	$P_4$	-73.9	1135.0
Coupler orientation		$P_1/P_1$	$P_2/P_2$	$P_3/P_3$	$P_4/P_4$
		$78^\circ$	$82^\circ$	$87^\circ$	$87.5^\circ$

The coordinates for precision points are given in mm

**Four-Bar Synthesis: Four-Position Motion Generation Procedure**

The kinematic synthesis of the planar mechanism is of three types: function generation from input links to output links, path generation of a point on a floating link that traces a predetermined path, and motion generation that guides a rigid body through a prescribed motion sequence. In our problem, a mechanism must be synthesized whose follower must provide support at the elbow and follow the trajectory of the elbow. This problem can be classified as a motion generation problem, as the coupler link must follow predetermined positions and orientations. A four-position motion generation method is used to synthesize the desired four-bar mechanism. A detailed explanation of this method can be found in the classical book Sandor and Erdman [35]. A brief description of the four-position motion synthesis is given here.

$ABCDE$  is the four-bar mechanism as shown in Fig. 4 a.  $AE =$  link 1,  $AB =$  link 2,  $BD =$  link 3,  $DE =$  link 4, and  $C$  is the coupler point that passes through four points  $C_1, C_2, C_3, C_4$ . Coupler position  $C_1$  is the reference position. The four-bar can be divided into two dyads  $WZ$  derived from  $AB$  and  $BC$ , and dyad  $US$  derived from  $ED$  and  $DC$ . Now consider only one-half of the four-bar mechanism  $WZ$  dyad. The reference position of the consecutive coupler positions  $C_2, C_3, C_4$  with respect to the reference point  $C_1$  can be given by the vector notation  $\delta_2, \delta_3, \delta_4$ , respectively. Vector  $W$  and  $Z$  make angles of  $\beta_2, \beta_3, \beta_4$  and  $\alpha_2, \alpha_3, \alpha_4$ , respectively, with the initial configuration of the four-bar. The loop closure equation at  $j^{th}$  configuration can be expressed by Eq. 1.

$$W(e^{i\beta_j} - 1) + Z(e^{i\alpha_j} - 1) = \delta_j \tag{1}$$

The three equations for coupler positions ( $j = 2, 3, 4$ ) are given in Eq. 2:

$$\begin{aligned} W(e^{i\beta_2} - 1) + Z(e^{i\alpha_2} - 1) &= \delta_2 \\ W(e^{i\beta_3} - 1) + Z(e^{i\alpha_3} - 1) &= \delta_3 \\ W(e^{i\beta_4} - 1) + Z(e^{i\alpha_4} - 1) &= \delta_4 \end{aligned} \tag{2}$$

In the four-position motion generation problem, the positions and orientation of the coupler  $BC$  are known. Therefore,  $\delta_2, \delta_3, \delta_4$  and the corresponding coupler angles  $\alpha_2, \alpha_3, \alpha_4$  are known. These three vector equations in Eq. 2 signify six scalar equations. The unknowns of these equations are two vectors  $W, Z$  and three angular positions  $\beta_2, \beta_3, \beta_4$ . For this system, the total number of unknowns is 7, and the total number of equations is 6. Thus, we have one free choice for the unknowns. For this problem,  $\beta_2$  is chosen as the free variable. The system can be solved for six unknowns  $W$  and  $Z$  and the angles  $\beta_3, \beta_4$ . The system of equations in Eq. 2 are

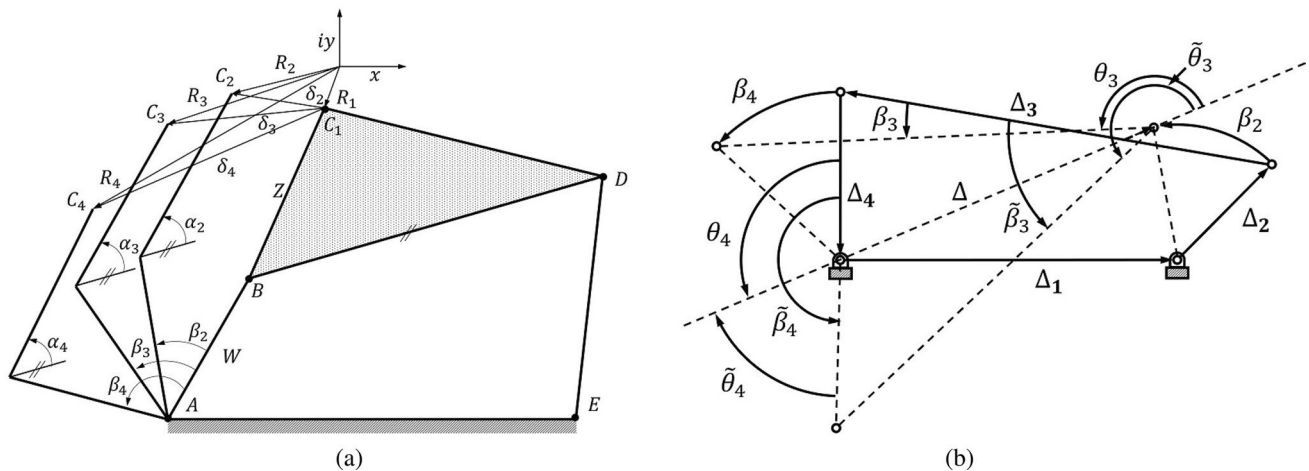


**Fig. 4** Four-bar synthesis. **a** Four-position motion generation problem. **b** Graphical representation of the compatibility equation (Eq. 5) for the unknown angles  $\beta_j, j = 3, 4$

nonlinear transcendental in  $\beta_3$  and  $\beta_4$ . The matrix form of Eq. 2 is given in Eq. 3:

$$\begin{bmatrix} e^{i\beta_2} - 1 & e^{i\alpha_2} - 1 \\ e^{i\beta_3} - 1 & e^{i\alpha_3} - 1 \\ e^{i\beta_4} - 1 & e^{i\alpha_4} - 1 \end{bmatrix} \begin{bmatrix} W \\ Z \end{bmatrix} = \begin{bmatrix} \delta_2 \\ \delta_3 \\ \delta_4 \end{bmatrix} \tag{3}$$

The right side and the second column on the left side of the coefficient matrix in Eq. 3 contain the required input values, whereas the first column has unknown rotations  $\beta_3$  and  $\beta_4$ . If the rank of the ‘‘augmented matrix’’ of the coefficients is 2, the system will have a solution. The necessary condition for this system to have a solution is that the determinant of this augmented matrix must be equal to zero. The determinant of this augmented matrix is shown in Eq. 4:

$$\begin{vmatrix} e^{i\beta_2} - 1 & e^{i\alpha_2} - 1 & \delta_2 \\ e^{i\beta_3} - 1 & e^{i\alpha_3} - 1 & \delta_3 \\ e^{i\beta_4} - 1 & e^{i\alpha_4} - 1 & \delta_4 \end{vmatrix} = 0 \tag{4}$$

Eq. 3 may be solved for the two scalar unknowns,  $\beta_3$  and  $\beta_4$ , as it is a complex equation having two independent scalar equations. Expanding the determinant about its first column,

$$\Delta_2 e^{i\beta_2} + \Delta_3 e^{i\beta_3} + \Delta_4 e^{i\beta_4} + \Delta_1 = 0 \tag{5}$$

where,

$$\Delta_1 = -\Delta_2 - \Delta_3 - \Delta_4 \tag{6}$$

and the expressions for the co-factors of the elements in the first column are the  $\Delta_j$ , ( $j = 2, 3, 4$ ) are

$$\Delta_2 = \begin{vmatrix} e^{i\alpha_3} - 1 & \delta_3 \\ e^{i\alpha_4} - 1 & \delta_4 \end{vmatrix}, \Delta_3 = - \begin{vmatrix} e^{i\alpha_2} - 1 & \delta_2 \\ e^{i\alpha_4} - 1 & \delta_4 \end{vmatrix}, \Delta_4 = \begin{vmatrix} e^{i\alpha_2} - 1 & \delta_2 \\ e^{i\alpha_3} - 1 & \delta_3 \end{vmatrix} \tag{7}$$

The variables are in exponential forms in the compatibility equation (Eq. 5). For computer implementation, this transcendental equation can be more simplified as

$$\Delta_3 e^{i\beta_3} + \Delta_4 e^{i\beta_4} = -\Delta \tag{8}$$

in which,

$$-\Delta = -\Delta_1 - \Delta_2 e^{i\beta_2} \tag{9}$$

Eqs. 8 and 9 can be easily understood with the help of graphical representation. For any value for  $\beta_2$ , values of  $\Delta$ ,  $\Delta_3$ , and  $\Delta_4$  are known. From Fig. 4, it is concluded that for any arbitrary value for  $\beta_2$ , there are two solutions for  $\beta_3$  and  $\beta_4$  and these pair of solutions can be written as  $(\beta_3, \beta_4)$  and  $(\tilde{\beta}_3, \tilde{\beta}_4)$ . These two sets of values are known as Burmester point pairs (BPPs). From Eqs. 8, 9 and Fig. 4b, expressions for the  $\beta_3, \tilde{\beta}_3, \beta_4, \tilde{\beta}_4$  are obtained as:

$$\begin{aligned} \beta_3 &= \arg \Delta + \theta_3 - \arg \Delta_3 \\ \tilde{\beta}_3 &= \arg \Delta + \tilde{\theta}_3 - \arg \Delta_3 \\ \beta_4 &= \arg \Delta + \theta_4 - \arg \Delta_4 \\ \tilde{\beta}_4 &= \arg \Delta + \tilde{\theta}_4 - \arg \Delta_4 + \pi \end{aligned} \tag{10}$$

in which,

$$\begin{aligned} \cos \theta_3 &= \frac{\|\Delta_4\|^2 - \|\Delta_3\|^2 - \|\Delta\|^2}{2\|\Delta_3\|\|\Delta\|} \\ \sin \theta_3 &= (1 - \cos \theta_3^2)^{1/2} \\ \tilde{\theta}_3 &= 2\pi - \theta_3 \\ \cos \theta_4 &= \frac{\|\Delta_3\|^2 - \|\Delta_4\|^2 - \|\Delta\|^2}{2\|\Delta_4\|\|\Delta\|} \\ \sin \theta_4 &= (1 - \cos \theta_4^2)^{1/2} \\ \tilde{\theta}_4 &= 2\pi - \theta_4 \end{aligned} \tag{11}$$

In Eq. 11, the values for  $\theta_3, \tilde{\theta}_3, \theta_4, \tilde{\theta}_4$  can be easily calculated, as these are functions of  $\Delta, \Delta_3$ , and  $\Delta_4$  only. Any two  $\beta$ 's from either of two sets,  $(\beta_2, \beta_3, \beta_4)$  and  $(\beta_2, \tilde{\beta}_3, \tilde{\beta}_4)$ , may be inserted into two of the three standard-form equations (refer Eq. 2). The solution for  $W$  and  $Z$  can be obtained by solving this linear system of equations. After finding the values for  $W$ , and  $Z$ , the circle point ( $K$ ) and center point ( $M$ ) can be found by using Eqs. 12:

$$\begin{aligned} K &= R - Z \\ M &= K - W \end{aligned} \tag{12}$$

The advantage of using the circle and the center points is that if we vary  $\beta_2$  from 0 to  $2\pi$  in steps, then we can plot the circle-point and centre-point curves and we will have multiple solutions for a single problem. Based on the design criteria, two circle points and corresponding centre points are chosen for the final solution.

### Four-Bar Mechanism Synthesis and Link Lengths

The starting position is chosen to be the sit-off position. The sit-off position is shown as point  $P_1$  in Fig. 3b. The point  $P_4$  is chosen at the extreme position of the elbow trajectory. The intermediate points  $P_2$  and  $P_3$  are chosen before and after the dip of the elbow trajectory iteratively to achieve an acceptable solution. For having an acceptable solution, the coordinates of points  $P_2, P_3$ , and  $P_4$  are changed by small distances based on the following analysis. In the case of four-position mechanism synthesis, the number of scalar equations is 6; the total number of scalar unknowns is 9; the number of free choices is 3, and the number of possible solutions is  $\mathcal{O}(\infty)^2$ . We consider the coupler angular rotations ( $\alpha$ 's) in the corresponding three rotations from the initial position to be the free choices as shown in Fig. 4a. The choice of  $\alpha$ 's depends on the desired orientation of the

coupler. As the coupler supports the patient during STS motion, the coupler should be positioned vertically during the operation. For keeping the values of  $\alpha$ 's to zero, the location of the synthesized device's ground pivots turns

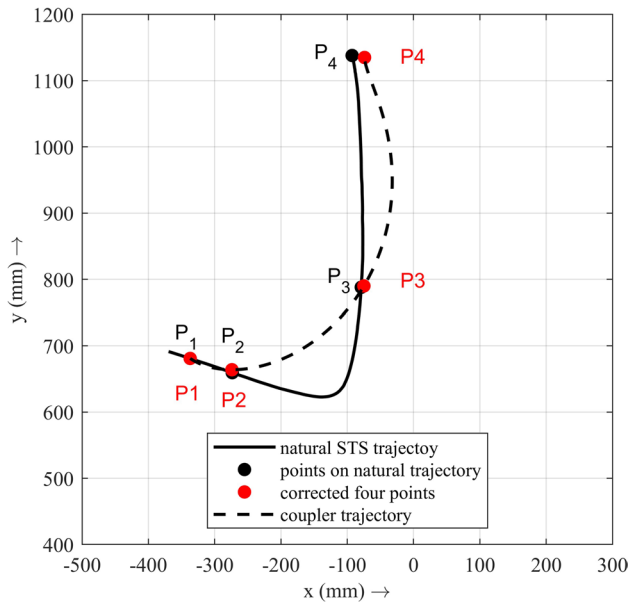


**Fig. 5** STS trajectory and coupler curve of synthesized four-bar. The synthesized precision points  $P_1, P_2, P_3, P_4$  do not exactly match with the targeted precision points  $P_1, P_2, P_3, P_4$  on STS trajectory, but differ by small margins. The exact values are given in Table 1

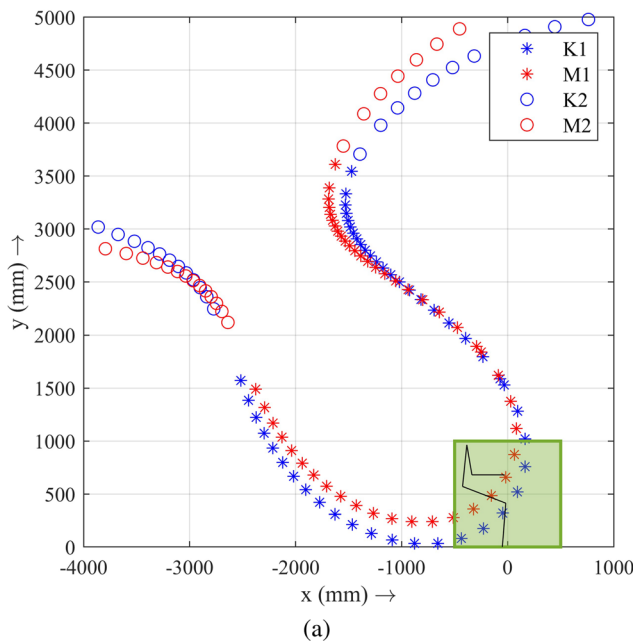
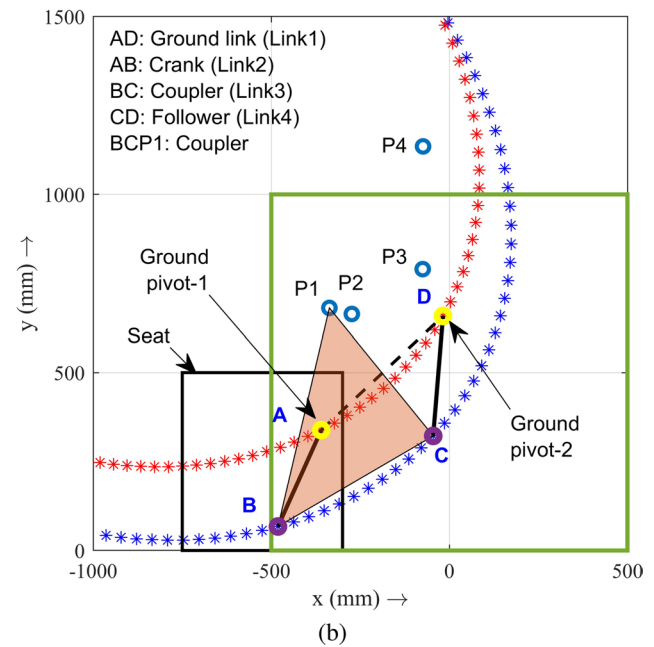


**Fig. 6** *K-M* plots and synthesized for-bar. **a** The plot of *K-M* curves. For each  $\beta_2$ , there are two possible sets of solutions for *K-M* points (Eq. 12). The design region is visualized using the green area

out to be far away from the chair. To find the possible set for acceptable values of  $\alpha$ , the angle is varied from  $0^\circ$  to  $10^\circ$  with a step size of  $0.5^\circ$ . All possible combinations of  $\alpha_2, \alpha_3, \alpha_4$  are found out. A single *K-M* plot is shown in Fig. 6a for  $\alpha_2 = 4^\circ, \alpha_3 = 9^\circ, \alpha_4 = 9.5^\circ$ . The initial angular configuration of the coupler is  $78^\circ$ . The highlighted green region in Fig. 6a (1000 mm $\times$ 1000 mm, starts 200 mm behind from the ankle as human faced at positive x-direction), is the preferred region for designing the mechanism.

The *K* and *M* curves are then plotted using the four updated prescribed coordinates ( $P_1, P_2, P_3, P_4$ ) and the angular positions listed in Table 1. These new points for the synthesis problem are shown in Fig. 5. The ground pivots closest to the seat are picked, as seen in Fig. 6a and b. The dimension of the coupler is  $BP_1$  and  $CP_1$ , and the link lengths of the mechanism are  $AB, BC$ , and  $CD$  are derived from the selected *K* and *M* points. Table 2 provides the dimensions of the links (roundoff values and unit is in mm).

Figure 7 shows the plot of  $\beta_3, \beta_4, \tilde{\beta}_3, \tilde{\beta}_4$  versus  $\beta_2$ . It is noted that there are no values of  $\beta_3, \beta_4, \tilde{\beta}_3, \tilde{\beta}_4$  between  $66^\circ < \beta_2 < 300^\circ$ . This demonstrates that for this range of  $\beta_2$ , the “compatible linkage” does not exist. The flexibility to select dyads in which the link *W* (refer Fig. 4) demonstrates a consistent directional rotation between precision points 1 to 4 is another useful design feature of this visualization. For instance, the solution corresponding to  $\beta_2 = 10^\circ$  has a constant directional rotation with  $\beta_3 = 50^\circ$  and  $\beta_4 = 109^\circ$  (see Fig. 7). The solution for the dyads of the linkage for



(1000 mm $\times$ 1000 mm). **b** *ABCDE* is the synthesized mechanism. *BCP1* is the coupler. The coupler points  $P_1$  trace the four precision points

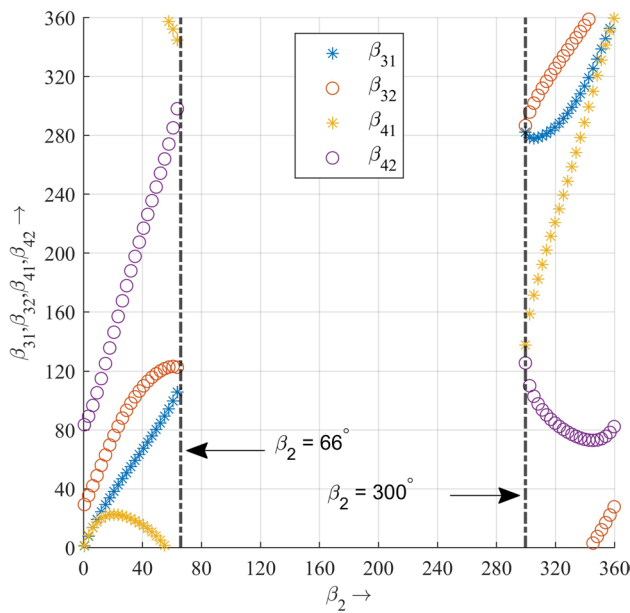


**Fig. 7** Plot of  $\beta$ 's verses  $\beta_2$ . The values for  $\beta_{31}$ ,  $\beta_{32}$ ,  $\beta_{41}$ , and  $\beta_{42}$  are solved for the corresponding value of  $\beta_2$  by using Eqs. 10 and 11

**Table 2** Four-bar link and frame dimensions

Link lengths	
Ground link length (link 1)	335 mm
Crank length (link 2)	200 mm
Coupler length (link 3)	330 mm
Follower length (link 4)	200 mm
Vertical link length (link 5)	510 mm

this motion generation problem is shown in Fig. 6b, and the coupler curve traced by this mechanism is shown in Fig. 5 (black dotted line). The total angular travel of the input link is  $150^\circ$ . The longest to shortest link length ratio for the four bar linkage in the STS device is 2.1.

### Optimal Trajectory During Assistive STS Motion and Support Reaction Force Calculation

The main objective of the STS assistive device is to reduce the effort by the user during STS transfer. The magnitude of the joint torques give an estimate of the effort given by the user during STS transfer. However, the joint torques cannot be measured directly. Hence, we develop an optimization model to find joint torques and external forces. Instead of experimental methods, numerical optimization techniques are used to find the external forces acting on the human body applied by the assistive device during sit-to-stand transfer. The device provides support at the elbow, armpit, hip and knee.

Armpit support is provided to maintain body posture during STS transfer. Knee support is provided to prevent feet from slipping on floor. An optimization problem is formulated to calculate the support reaction forces. The magnitudes of the support forces and the ankle, knee, hip, shoulder and elbow joint angles are the variables of this problem. Since STS transfer is considered to be symmetric about the sagittal plane, and the support device will also apply symmetric reactions. Due to this reason, our simplified human multibody system model consists of five segments, including the shank, thigh, torso, upper arms, and forearms. The left and right arm and leg segments are combined to consider the total body segment weights of the human. The head is combined with the torso. The foot portion is removed, and appropriate constraints are applied to maintain contact with the ground. The model is powered by five torque actuators at the ankle, knee, hip, shoulder, and elbow. Dynamic model equations have been set up using the efficient multibody dynamics algorithm based on the Newton-Euler recursive formula as given in the book by Ghosal [16]. All the body segment parameters required for the model are calculated by using anthropometric data provided in De Leva [13]. Here, a mathematical model is developed to represent the STS motion, where the patient is lifted from the chair and partially supported by external forces as they stand up. The multibody dynamics equation is of the form given in Eq. 13:

$$\mathcal{M}(\theta)\ddot{\theta} + \mathcal{N}(\theta, \dot{\theta})\dot{\theta} + \mathcal{G}(\theta) = \mathcal{T} + \mathcal{T}_{\text{ext}} \tag{13}$$

The vectors of positions and velocity variables are defined as  $\theta$  and  $\dot{\theta}$ . The body mass matrix is defined by  $\mathcal{M}(\theta)$ . The centripetal and Coriolis terms are represented by  $\mathcal{N}(\theta, \dot{\theta})$ . The gravity terms are denoted by  $\mathcal{G}(\theta)$ . The right-hand side of Eq. 13 represents the sum of all forces and moments.  $\mathcal{T}$  represents the generalized actuation forces, and  $\mathcal{T}_{\text{ext}}$  denotes the generalized support reaction forces acting on the body due to the assistive device. The specifications of  $\mathcal{T}_{\text{ext}}$  include the quantity and locations of its insertion at the hip, below the knees, at the armpit, and at the elbow. The force insertion points are set with respect to the body segment, but optimization will define the magnitudes and direction of these forces. The objective is to provide limited support during motion up to a specific percentage of body weight, in this case, up to 50% of body weight in the vertical direction.

The optimization problem formulated is an optimal control problem based on the mechanical model of human multibody dynamics described above. The problem is formulated as shown in Eq. 14:



$$\min_{\tau_{\text{ext}}, \theta} \int_{t=t_0}^{t=t_f} \left( \sum_{i=1}^{n_{\text{act}}} (\alpha \tau_i^2 + \beta |\tau_i \dot{\theta}_i|) + \delta \sum_{k=1}^{n_{\text{ext}}} \tau_{\text{ext},k}^2 \right)$$

subjected to: Equations of motion, and

$$\theta(t = t_0) = \theta_{\text{ini}}$$

$$\theta(t = t_f) = \theta_{\text{end}} \tag{14}$$

$$\theta^{lb} \leq \theta \leq \theta^{ub}$$

$$\tau_{\text{ext}}^{lb} \leq \tau_{\text{ext}} \leq \tau_{\text{ext}}^{ub}$$

$n_{\text{act}} = 5$  (number of joints considered)

$n_{\text{ext}} = 8$  (number of support forces)

$\theta(t)$  denotes the angular orientation of ankle, knee, hip, shoulder, and elbow joints.  $\tau(t)$  defines the joint torques. It includes the combined effect of the left and right joints, and  $\tau_{\text{ext}}(t)$  defines the external forces.  $t_0$  and  $t_f$  defines the initial and final time, respectively. Open uniform quartic b-spline curve is used to model the joint trajectories. In a similar method, the support reaction forces are also defined. The control points of these b-spline functions are the variables of this optimization problem. The b-spline curve is chosen to ensure continuity, differentiability, and endpoint interpolation.

The objective function is shown in Eq. (14) and consists of a weighted combination of three terms that have been determined heuristically and create realistic behaviour of the subjects [26]. The first term represents the sum of the squared joint torque. The second term represents the sum of mechanical power expended in all joints, which is an important criterion for elderly or injured people. The last term is a regularization term (a term with low weight) to reduce the influence of external force on these primary criteria. The value for the weights  $\alpha$ ,  $\beta$ , and  $\delta$  are given in Mombaur and Hoang [26].

Equation (14) includes several additional constraints, such as lower and upper limits on all joint angles, angular velocities, forces and torques, restrictions on external forces, starting conditions (such as sitting position with arm posture correlated with support settings, and with no initial velocities), as well as end conditions (such as upright standing at rest with correlative support setting, with no final velocities). The total height and weight of the human model are 172 cm and 53 kg which corresponds to the healthy subject in experiment. The STS motion is initiated with a straight sitting pose and zero initial velocities. All the initial and final values for the design variables are given in Table 3. The lower and upper limits for the support reaction forces are given in Table 4. The limits for the support reaction forces are taken from Mombaur and Hoang [26].

## Actuator Selection, Frame Design and Fabrication

### Actuator Selection

During STS, the height difference in posture is mainly due to the change in orientation of the thigh bone or femur from horizontal to vertical, plus some effects due to the straightening of the lower leg and the spine. Since the average length of the human femur is approximately 436 mm [27], after giving allowances, we consider the vertical movement of the STS device (elbow support shown in Fig. 9c and d) to be 450 mm. A linear actuator is selected that can lift a 100 kg person and which displaces the support bar vertically by 450 mm. The linear actuator is mounted on both ends using pivot joints. One end of the actuator is connected to the end of the crank, and the other is connected to a mount fixed on the frame. This mounting method allows the actuator to pivot on both sides as the actuator extends or retracts. Two identical linear actuators are used to actuate the device for symmetric application. The specifications for the linear actuators are given in Table 5.

A rechargeable battery is used to power the actuators. The rechargeable battery specifications are 12 V, 7 Ah, and weight of 2.4 kg. The number of cycles that the linear actuator can run with a fully charged battery is approximately 100 cycles. These two actuators can operate simultaneously using a single DPDT switch.

### Frame Design and Device Fabrication

The frame of the device has been designed to support the mechanism and provide balance to the user during sit-to-stand motion. Aluminium 6063 profile of dimension (40 mm × 40 mm) was used to fabricate the frame and mechanism links to keep the device lightweight and durable. The STS device has identical four-bar mechanisms mounted on both sides of the frame, with one actuator to operate on each side as shown in Fig. 8a. A static structural analysis (using Abaqus® simulation software) of the frame and links was performed to check the elastic deformation under load application. During stress analysis, 50 kg load was applied on each side of the frame. In static finite element analysis, the links were modeled as simply supported with vertical loads, and the frame had a fixed boundary condition on the lower horizontal base with vertical load acting on the top. The maximum von Mises stress in different links are shown in Table 6. The fabricated device is shown in Fig. 9. The total weight of the frame is 18 kg. A harness is attached to the support bar to provide extra support at the back of the thigh, as shown in Fig. 9b. The user’s centre of gravity lies within the base of the device and prevents falling. To incorporate the usability of the device for users of different heights, a height adjustment mechanism is incorporated in the device

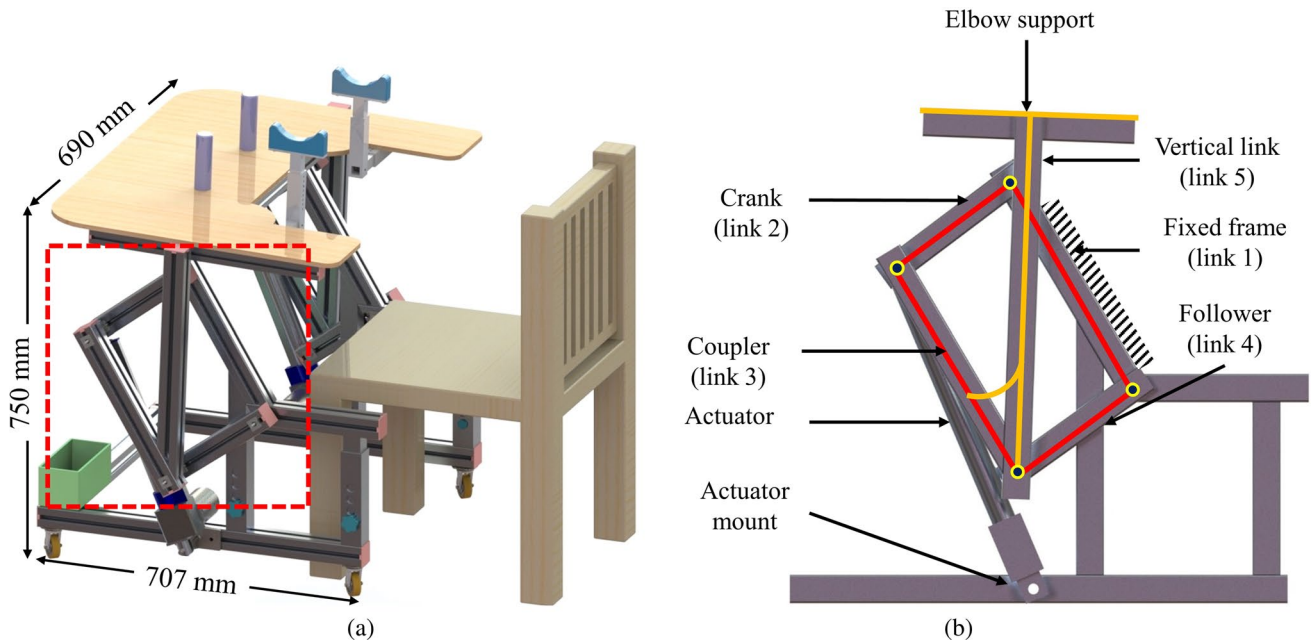


**Fig. 8** **a** STS device in ready-for-use position (CAD model). The four-bar mechanism is outlined with a dashed red box. **b** Side view of the four-bar mechanism in the STS device. The kinematic diagram of

the four-bar is shown in red lines, and the coupler extension is shown using yellow lines

**Table 3** Initial and final values for the design variables

Initial values		Final values	
$t = t_0$	0 s	$t = t_f$	70 s
$\theta^{\text{ankle}}(t = t_0)$	$70^\circ$	$\theta^{\text{ankle}}(t = t_f)$	$70^\circ$
$\theta^{\text{knee}}(t = t_0)$	$0^\circ$	$\theta^{\text{knee}}(t = t_f)$	$0^\circ$
$\theta^{\text{hip}}(t = t_0)$	$90^\circ$	$\theta^{\text{hip}}(t = t_f)$	$90^\circ$
$\theta^{\text{shoulder}}(t = t_0)$	$0^\circ$	$\theta^{\text{shoulder}}(t = t_f)$	$0^\circ$
$\theta^{\text{elbow}}(t = t_0)$	$60^\circ$	$\theta^{\text{elbow}}(t = t_f)$	$60^\circ$

**Table 4** Lower and upper limits for the horizontal and vertical components of the support reaction forces

Horizontal component (N)	Vertical component (N)
$-50 \leq \tau_x^{\text{ankle}} \leq 0$	$-5 \leq \tau_y^{\text{ankle}} \leq 5$
$0 \leq \tau_x^{\text{thigh}} \leq 175$	$0 \leq \tau_y^{\text{thigh}} \leq 550$
$0 \leq \tau_x^{\text{armpit}} \leq 100$	$0 \leq \tau_y^{\text{armpit}} \leq 150$
$0 \leq \tau_x^{\text{elbow}} \leq 20$	$0 \leq \tau_y^{\text{elbow}} \leq 50$

**Table 5** Linear actuator specifications

Self locking force	6000 N
Stroke length	300 mm
Speed at full load	$5 \text{ mm s}^{-1}$
Mounting length	500 mm
Voltage	12 V

**Table 6** Maximum von Mises stresses at different links of mechanism

Links	Maximum von Mises stress
Crank	12.9 MPa
Follower	41.73 MPa
Coupler	91.26 MPa
Frame	19.6 MPa

by means of locking two adjacent profiles, which is shown in Fig. 9a. The overall length, width, and height of the device are 700 mm, 600 mm, and 850 mm, respectively. The device is mounted on four castor wheels with a base height from the ground is 80 mm.

## Simulation and Experiment Results

### Optimization-Based Simulation

The position, velocity profiles, joint torques, and external forces are calculated by formulating an optimal control problem given in Eq. 14. Angles of the ankle, knee, hip, shoulder, and elbow joints and support reaction forces are the variables of this optimal control problem. The time considered for this optimization problem is 70 s since the device takes the same amount of time to complete the

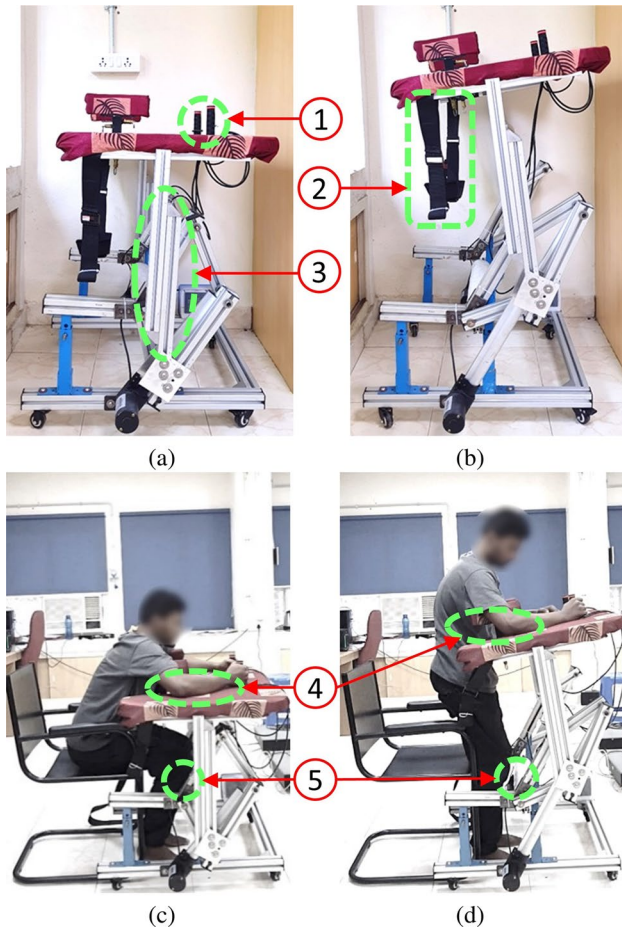


**Fig. 9** **a** The fabricated assistive device is shown in the seated position. **b** The assistive device is shown in a standing position. **c** The user with the device is in a sitting position. **d** The user with the device is in a standing position. Some device components are labelled here. (1) Grab bar: During operation, the user holds the grab bar. (2) Harness: It provides support at the back of the thigh of the user. The harness is hanging from the elbow support, and the length of the harness is adjustable. (3) Height adjustable mechanism: The two components can slide over each other and be kept fixed at a required position. (4) Elbow support: During the operation, the user places their elbow on this elbow support part. (5) Knee support: It provides support to the knee during STS motion

operation. Figure 10 shows motion sequence snapshots of the STS motion. The green arrows indicate the external forces acting on the human model. The direction and size of the arrows represent the relative magnitudes and directions of the support reaction forces. In Fig. 11, the support forces are plotted for all support points, i.e., at the knee, back of thigh, armpit and elbow. Note that the force results represent the combined forces exerted on both sides of the body. The motion of the force insertion point below the knee is minimal, considering that the heel is assumed to maintain contact with the ground throughout the motion, and the leg transitions from a bent position to a stretched position. Forces acting in the horizontal (X) direction at

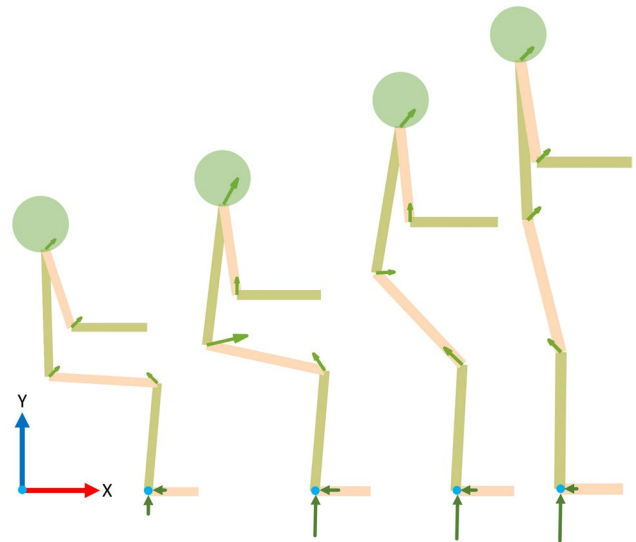


**Fig. 10** Snapshots of the optimal STS motions for support scenarios. The arrows depict the directions and relative magnitudes of the forces exerted on the human body by the device

the knee prevent the patient from slipping. The forearms are kept maintaining a horizontal configuration. In this scenario, the vertical force exerted on the patient’s armpit is restricted to 100 N. The idea behind this limitation is to ensure that the primary force on the trunk is directed forward, and the required vertical force should be generated through friction without a tight grip on the grab bar of the device. The arms play a substantial role in distributing the force, which should remain within the feasible range for patients. An interesting observation is that this

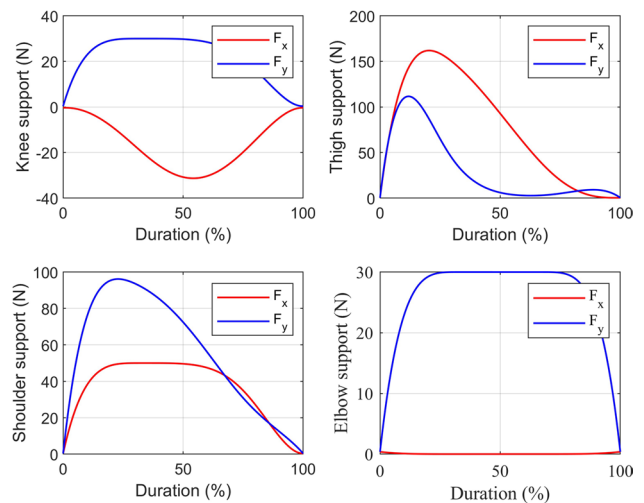


**Fig. 11** Optimization results for knee, thigh, armpit and elbow support forces in horizontal and vertical directions. Vertical and horizontal force components are shown using red and blue lines, respectively

force distribution makes it feasible to support sit-to-stand transfers with only minimal vertical forces at the trunk.

### Sit-to-Stand Experiment with Assistive Device

STS experiments were conducted on a force plate with 10 healthy male volunteers. During experiments, on average 42% reduction in GRF force was recorded while using STS assistive device. Here, the STS experiment data of a male subject of height 172 cm and weight 53 kg is presented in Fig. 12. The GRF during natural STS motion and assistive STS motion with the fabricated device is shown in Fig. 12b. The natural STS motion takes approximately 3 s to complete. The initial 1–2 s is the reaction force of feet. The lift-off from the seat approximately starts at 2.2 s. At this instant of time, a dip in the GRF is recorded. Then, a sudden rise in the GRF can be seen as the human rapidly stands up. Then, some extra time is required for the force plate reading to stabilise to the weight of the human (53 kg). The unassisted STS motion is showed using a solid line in Fig. 12b and the maximum GRF (547 N) is marked with a red circle in the same. The total time of the STS motion with the assistive device is much longer (approximately 70 s) compared to natural STS motion. Here again, initially, we get the reaction force of feet. Then, approximately at 10 s, the STS device is actuated, and the human is slowly moved from sitting to standing position. At approximately 15 s is the lift-off from the seat, so the load on the feet increases. This load slowly increases and stabilizes at approximately 520 N. Hence, approximately 230 N load is taken by the assistive device during STS motion. Finally, around 70 s, the person is completely in a standing position. Hence, the load on his feet increases to full body weight. Therefore, the load borne by the assistive device during STS motion is approximately 45%.

The optimal trajectory of the human body segments during the assistive STS motion is calculated using the optimization method. The optimal trajectory of the shoulder and elbow and four positions  $P1$ ,  $P2$ ,  $P3$ , and  $P4$  are shown in Fig. 12a. The positions  $P1$  and  $P4$  are the sitting and standing positions, whereas  $P2$  and  $P3$  are the intermediate positions during the STS motion. The support reaction forces and ground reaction forces are calculated using optimization at these four positions are given in Table 7. The error percentages calculated between experimental GRF and calculated GRF from optimization are also given in Table 7. Figure 10 shows relative magnitude and direction of these forces with arrows. The variations can be attributed to various factors, such as limitations in the optimization model or inaccuracies in data collection during experiments.

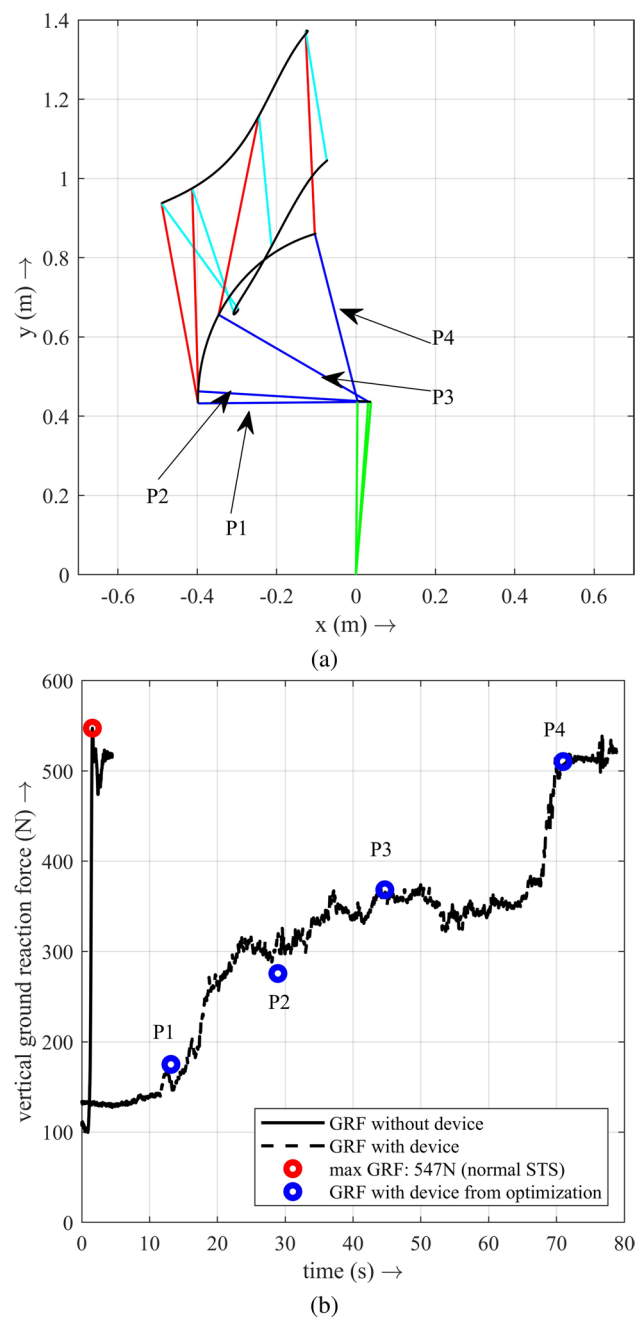


**Fig. 12** **a** Intermediate snapshots of STS transfer from optimization. The initial and final positions are  $P1$ ,  $P4$ , and  $P2$ ,  $P3$  are the intermediate positions. The optimal trajectory of the shoulder and elbow are shown using black curves. **b** Ground reaction force (GRF) data recorded from the assistive STS experiment. The solid curved is GRF without STS device; the dashed curve is for STS with assistive device. The maximum GRF during un-assisted STS is shown with a red circle. GRF data calculated from optimization at positions  $P1$ ,  $P2$ ,  $P3$ ,  $P4$  is shown using blue circles

**Table 7** Support and ground reaction forces calculated using optimization corresponding to the positions *P1, P2, P3, P4* shown in Fig. 12a

Position	Knee support		Thigh support		Armpit support		Elbow support		Vertical GRF		% error in GRF
	$F_x$	$F_y$	$F_x$	$F_y$	$F_x$	$F_y$	$F_x$	$F_y$	calculated	experiment	
<i>P1</i>	-3.31	28.13	160.16	48.24	46.88	92	0.013	28.13	175	156.94	11.51
<i>P2</i>	-12.83	29.98	141.33	9.17	49.99	84.53	0.0041	29.99	275.68	310.41	11.19
<i>P3</i>	-14.06	29.07	81.2	6.611	48.49	55.22	0.007	29.99	368.41	363.62	1.32
<i>P4</i>	0.554	5.92	15.03	19.96	9.84	11.42	0.0571	22.81	510.39	507.84	0.5

The percentage error in GRF from experiments at these four positions is shown in last column. All the forces are given in N

### Discussions and Conclusion

This paper presented the design and development of an assistive device that helps in STS motion following natural trajectory. The summary of the design procedure is as follows: (i) Obtain STS natural trajectories by performing experiments on healthy volunteers; the elbow trajectory is traced. (ii) Using Burmester curve theory and four point motion generation synthesis procedure, a coupler curve for the four-bar mechanism is generated that closely follows the natural STS trajectory. (iii) By trial and iteration the ground pivots of the four-bar mechanism is selected based on allowable zones and link lengths are determined. (iv) Frame housing the four-bar mechanism and its linear actuators is designed based on structural stability and strength requirements. (v) Frame design incorporated height adjustment mechanism for different users and provide support to the user at knee, back of thigh, and elbow to ensure that user’s body weight is well-distributed between support points and there is no slip at feet.

In this work, linear actuators are used which are relatively slow than programmable high torque DC servo motors; however, linear actuators can provide high thrust force, have good positional accuracy, can be easily actuated and controlled, and are low in cost. Since, the STS device is for use of old and infirm whose motions are slow, we feel that linear actuators are suitable for actuation. Actually, one single linear actuator provides sufficient thrust force to lift a person of even more than 100 kg weight. Our previous work [11] provided support at one shoulder for aiding STS. However, since the body weight was not evenly distributed, the volunteers gave feedback that STS device was not comfortable, and hence in the design proposed in this work, two linear actuators are used, as well as arm rest, knee and thigh support for symmetric and even distribution of body weight.

The STS device was fabricated and tested on healthy volunteers. While the device can be easily actuated by pressing a switch, it was noted that tying the belt for thigh support single-handed may not be easy for some users. It was also observed that the elbow rest tilts by approximately 5° as the

device moves from sit to stand position. Using optimization, the support contact forces were calculated and used to evaluate the GRF, which were compared with GRFs from experiments. A more direct approach might have been to use pressure sensors at support contact locations; but our opinion is that force plate measurements are more accurate than pressure sensors. The GRF comparison between optimization and experiment indicates that the calculated forces from the optimization model are within acceptable limits. Hence, a full computation model based on trajectory optimization that is used both for internal force prediction and synthesis of the STS mechanism as proposed in [31] can be developed. Future work will focus on these directions.

**Acknowledgements** The STS experiments with healthy volunteers were permitted under IIT Madras institute ethical committee (IEC) protocol number IEC/2021-01/SR/02. The authors would like to acknowledge PORTESCAP India Pvt Ltd. for funding fabrication of the STS device.

**Funding** The authors have not disclosed any funding.

### Declarations

**Competing interests** The STS device has been filed for Indian patent with provisional application number 202441012717.

### References

1. N. Abdul Ghani, M.O. Tokhi, Sit-to-stand and stand-to-sit control mechanisms of two-wheeled wheelchair. *J. Biomech. Eng.* **138**(4), 041007 (2016)
2. A. Asker, O. Salah, A.M.F. El-Bab, S.M. Assal, A.A. Ramadan, S. Sessa, A. Abo-Ismael, Development of parallel manipulator sit to stand assistive device for elderly people. in 2013 IEEE Workshop on advanced robotics and its social impacts, IEEE, pp. 27–32 (2013)
3. A. Asker, O. Salah, A.M.F. El-Bab, A.A. Ramadan, S.M. Assal, S. Sessa, A. Abo-Ismael, Anfis based jacobian for a parallel manipulator mobility assistive device. in 2014 UKACC International conference on control (CONTROL), IEEE, pp. 395–400 (2014)
4. A. Asker, S.F. Assal, A.M. Mohamed, Dynamic analysis of a parallel manipulator-based multi-function mobility assistive device

- for elderly. in 2015 IEEE International conference on systems, man, and cybernetics, IEEE, pp. 1409–1414 (2015)
5. R. Bostelman, J.C. Ryu, T. Chang, J. Johnson, S.K. Agrawal, An advanced patient lift and transfer device for the home. *J. Med. Devices* **4**(1), 11004 (2010)
  6. M.E. Boyce, H.E. Boyce, Convalescent aid. US Patent 4941495A (1990)
  7. F.H. Bratton, Patient riser. US Patent 3668723A (1972)
  8. D. Chugo, T. Asawa, T. Kitamura, S. Jia, K. Takase, A rehabilitation walker with standing and walking assistance. in 2008 IEEE/RSJ International conference on intelligent robots and systems, IEEE, pp. 260–265 (2008)
  9. M.D. Costello, Assisted lifting, stand and walking device. US Patent 5502851A (1996)
  10. T.W. Cunningham, Rising brace for invalid walker. US Patent 5005599A (1991)
  11. S. Das, S. Halder, S.K. Sahu, S. Srinivasan, S. Rakshit, Design and development of a sit-to-stand assistive device, in *Machines*. (Springer, Mechanism and Robotics, 2022), pp.249–256
  12. K.G. Davis, S.E. Kotowski, Prevalence of musculoskeletal disorders for nurses in hospitals, long-term care facilities, and home health care: a comprehensive review. *Hum. Factors* **57**(5), 754–792 (2015)
  13. P. De Leva, Adjustments to zatsiorsky-seluyanov's segment inertia parameters. *J. Biomech.* **29**(9), 1223–1230 (1996)
  14. L.T. D'Angelo, K. Abdul-Sater, F. Pfluegl, T.C. Lueth, Wheelchair models with integrated transfer support mechanisms and passive actuation. *J. Med. Devices* **9**(1), 11012 (2015)
  15. A. Fattah, S.K. Agrawal, G. Catlin, J. Hamnett, Design of a passive gravity-balanced assistive device for sit-to-stand tasks. *J. Mech. Des.* **128**(5), 1122–1129 (2005). <https://doi.org/10.1115/1.2216732>
  16. A. Ghosal, *Robotics: Fundamental Concepts and Analysis* (Oxford University Press, 2006)
  17. K. Goher, M. Shafiq, A. Al-Yahmadi, Design of a reconfigurable wheelchair with a sit-to-stand facility for a disabled kid. in Nature-inspired mobile robotics, world scientific, pp. 133–140 (2013)
  18. R. Hakamiun, D.P. Genereux, M.D. Falin, M.J. Mutka, J.C. Brooke, Stand assist lift. US Patent 6175973B1 (2001)
  19. E.S. Howle, Foldable walker. US Patent 6311708B1 (2001)
  20. R.M. Kauffman, Prosthetic device for lifting and lowering a person thereon. US Patent 5265689A (1993)
  21. Kim Hg, S. Park, C. Han, Design of a novel knee joint for an exoskeleton with good energy efficiency for load-carrying augmentation. *J. Mech. Sci. Technol.* **28**(11), 4361–4367 (2014)
  22. S.W. Kim, J. Song, S. Suh, W. Lee, S. Kang, Design and experiment of a passive sit-to-stand and walking (stsw) assistance device for the elderly. in 2018 40th Annual international conference of the IEEE engineering in medicine and biology society (EMBC), IEEE, pp. 1781–1784 (2018)
  23. R. Kumar, Senior Citizen—Status in India. <https://vikaspedia.in/InDG> (2022)
  24. J. Kuželický, M. Žefran, H. Burger, T. Bajd, Synthesis of standing-up trajectories using dynamic optimization. *Gait Posture* **21**(1), 1–11 (2005)
  25. Y. Marcoux, A. Veilleux, Lift chair. US Patent 6213554B1 (2001)
  26. K. Mombaur, K.L.H. Hoang, How to best support sit to stand transfers of geriatric patients: motion optimization under external forces for the design of physical assistive devices. *J. Biomech.* **58**, 131–138 (2017)
  27. S.S. Moosa, M.H.R. Shaikh, M. Khwaja, S.A.H. Shaikh, F.B. Siddiqui, S.R.H. Daimi, S.D. Hiware, E.E. Ismail, Y. Begum, Sexual dimorphic parameters of femur: a clinical guide in orthopedics and forensic studies. *J. Med. Life* **14**(6), 762 (2021)
  28. S. Nuzik, R. Lamb, A. VanSant, S. Hirt, Sit-to-stand movement pattern: a kinematic study. *Phys. Ther.* **66**(11), 1708–1713 (1986)
  29. M. Peshkin, D.A. Brown, J.J. Santos-Munné, A. Makhlin, E. Lewis, J.E. Colgate, J. Patton, D. Schwandt, Kineassist: A robotic overground gait and balance training device. in 9th International conference on rehabilitation robotics, 2005. ICORR 2005., IEEE, pp. 241–246 (2005)
  30. A. Purwar, T. Galeotafiore, J. Miles, J. Renert, Portable six-bar apparatus for lifting, lowering and self-propelled transit. US Patent 8468622B2 (2013)
  31. S. Rakshit, S. Akella, A trajectory optimization formulation for assistive robotic devices. in 2016 IEEE International conference on robotics and automation (ICRA), IEEE, pp. 2068–2074 (2016)
  32. D. Randall, D.R. Gill, Dual handed walking and uprisal assist device. US Patent 5785070A (1998)
  33. E. Razon, Sit down and stand up walker with seat assembly. US Patent 8151812B2 (2012)
  34. P. Rea, E. Ottaviano, G. Castelli, A procedure for the design of novel assisting devices for the sit-to-stand. *J. Bionic Eng.* **10**(4), 488–496 (2013)
  35. G.N. Sandor, A.G. Erdman, *Advanced mechanism design v. 2: Analysis and synthesis*. Prentice-Hall (1984)
  36. A.M. Trinkoff, J.A. Lipscomb, J. Geiger-Brown, B. Brady, Musculoskeletal problems of the neck, shoulder, and back and functional consequences in nurses. *Am. J. Ind. Med.* **41**(3), 170–178 (2002)
  37. B.W. Vanzant, Pneumatic sit/stand assistance device having improved stabilization features. US Patent 5742957A (1998)
  38. A.B. Wilson, Aid for use in sitting down or standing up. US Patent 3739793A (1973)
  39. M.A. Wolferts, Holder for invalid walker. US Patent 3085258A (1963)

**Publisher's Note** Springer Nature remains neutral with regard to jurisdictional claims in published maps and institutional affiliations.

Springer Nature or its licensor (e.g. a society or other partner) holds exclusive rights to this article under a publishing agreement with the author(s) or other rightsholder(s); author self-archiving of the accepted manuscript version of this article is solely governed by the terms of such publishing agreement and applicable law.